

Computer simulations on collision-sequence mechanisms: Bombardment of single-crystalline Cu(100) by Ar ions

J. Likonen

Technical Research Centre of Finland, Reactor Laboratory, Otakaari 3 A, SF-02150 Espoo, Finland

M. Hautala

Department of Physics, University of Helsinki, Siltavuorenpenger 20 D, SF-00170 Helsinki, Finland

(Received 22 December 1989)

The development of collision-cascade anisotropies and the collision-sequence mechanisms in single-crystalline Cu are studied employing the binary-collision lattice-simulation code COSIPO and the distributions of the recoil vector fluxes. The vector fluxes are directly related to other statistical distribution functions of recoils and to the angular distributions of sputtered particles. Single-crystal Cu(100) is bombarded with normally incident 5-keV Ar ions. In addition to depth resolution of the recoil vector fluxes, the evolution of anisotropies is studied as a function of energy. The effect of various types of collision sequences on the fluxes may be treated separately. The collision cascade is found to be highly anisotropic at different depths and energies of recoils, and it is dominated by focusing along the $\langle 110 \rangle$ directions. The development of the collision cascade is entirely governed by crystal structure. A diversity of mechanisms responsible for creating the chains exists. The contributions of various collision chain mechanisms to recoil flux distributions and observed spot patterns are discussed. Thermal vibrations shorten the collision sequences and decrease the contribution of chains to the flux distributions, except in the case of defocused chains. Their fraction increases when thermal vibrations are included.

I. INTRODUCTION

Collision cascades are fundamental to many ion-solid interactions, such as radiation-induced defects, sputtering, and mixing. Analytical collision cascade theories usually make use of linearized transport equations of the Boltzmann type.^{1,2} It is usually assumed in these linear-cascade models that the cascade is dilute and has a large number of isotropically distributed low-energy recoil atoms. One of the basic assumptions is that of random target. The theory can be extended to cover anisotropy effects.³⁻⁸ In its region of validity, the linear-cascade theory has turned out to be highly successful in predicting qualitatively and quantitatively the experimentally measured sputtering data.

One of the basic limitations of the linear-cascade models is the omission of crystal structure. These theories neglect the fact that crystalline materials have a well-ordered structure and that the distributions of energy and momentum among the atoms in a collision sequence are influenced by this structure. In crystalline targets, correlated collision chains propagate effectively along or parallel to atomic rows and planes. The basic features of focused collision sequences were first proposed by Silsbee.⁹ He suggested that momentum can be focused in some cases so that collision chains can be used to transfer energy without mass. The transfer will continue either until all the energy is dissipated or the sequence strikes a discontinuity such as a surface. Nelson¹⁰ extended the focusing sequence mechanism to the case of thermally

vibrating atomic rows. Thompson has reviewed the basic physical mechanisms in sputtering and the analytical calculations of monocrystalline sputtering.¹¹

Recently Hou and Eckstein have studied qualitative aspects of momentum distributions in collision cascades in crystalline targets.¹² Quantitative features, such as the contributions of various collision sequences to these distributions and spot patterns, were not treated. No such calculations have been performed so far for recoil flux distributions. The fractions of different collision chain mechanisms have been studied quite extensively in several papers¹³⁻¹⁶ but only in connection with sputtering. Posselt¹⁷ has calculated the statistical distribution functions in amorphous targets using TRIM code in a similar way as in our previous papers.^{18,19} He investigated some characteristic features of the energy and directional distributions and compared the results of simulations to the analytical theory of Sigmund.²

In the previous paper²⁰ (to be referred to as "I" throughout this paper) in this series, emphasis was laid on presenting the method of calculations of the collision-cascade anisotropies in a single crystal and on the peculiarities caused by the crystalline structure. Energy transfer without mass transport in collision sequences was clearly observed. In this paper we continue this work and investigate different mechanisms during collision cascades more thoroughly and quantitatively than in our previous papers.¹⁸⁻²⁰ The same computational techniques are used that were described in I, except that the treatment of simultaneous collisions has been improved.

The main modification in the COSIPO code compared to the previous paper is that it enables both energy and depth resolution, whereas in I the method allowed only depth resolution. In addition to this modification the present version of COSIPO enables us to extract detailed information about the contributions of various collision chains to flux distributions and spot patterns. Discussion on different mechanisms in connection with sputtering will be continued in the final part III of the work.²¹ The obvious aim of the series of these studies is to form a background for future comparisons with analytical calculations of monocrystalline sputtering and possible improvements in them. Before doing that we need a good understanding of the basic mechanisms in cascades and sputtering.

II. METHOD OF CALCULATION

A. The computational model

We have used the COSIPO code²² with the following assumptions in the calculations.

(1) The procedure of binary and nearly simultaneous collisions is described elsewhere.^{20,23} The procedure was modified slightly and the impact parameter $b_{\max 2}$ was changed to $0.72a$ compared to those in paper I to better take into account the interactions with the ring atoms and the energy losses to the focusing rings around the crystal axes.²³ Otherwise the same parameters were used as in Ref. 23.

(2) The surface is represented by a planar barrier with the sublimation energy as surface binding energy $E_s=3.5$ eV.²⁴ To account for realistic lengths of collision sequences an amount of $E_b=0.2$ eV is subtracted from the kinetic energy of every atom leaving its lattice site.²⁵

(3) Inelastic energy losses are included using the Oen-Robinson model.²⁶ In the present paper electronic energy loss is taken into account when calculating the collision kinematics.²⁷

(4) The collision cascades are sufficiently dilute and can be regarded as linear. A target atom is displaced when recoiling with a kinetic energy larger than a threshold value E_d . The recoils in the cascades are followed until their energy falls below a threshold energy E_c . The threshold values E_c and E_d were chosen to be equal to the surface binding energy E_s .

(5) The interaction potential $V(r)$ is assumed to be a screened Coulomb potential with screening lengths suggested by Robinson,²⁷ the screening function is the Molière function. The screening lengths used are $a=0.089$ Å for Ar-Cu collision and $a=0.0739$ Å for Cu-Cu collision.

(6) Elastic scattering described by classical dynamics is assumed.

(7) The effects of mass transport by the recoil fluxes²⁸ are assumed to be negligible, and thus the density is constant. The cascades take place in a perfect crystal.

(8) Energy transport due to electronic cascade effects

is neglected.

(9) Thermal displacements are included by assuming that they are uncorrelated and Gaussian distributed. The target temperature is 300 K in the simulations. The root-mean-square displacement (0.08 Å) of the target atoms is based on the Debye model.

The implications of these assumptions have been discussed elsewhere.^{20,23} A detailed parameter study was performed in Ref. 23. The combination of the interaction potential and the electronic energy loss used in paper I gave a moderate agreement with experimental results. In this paper these parameters have been changed to give a better prediction of sputtering yields and angular distributions as shown in Ref. 23. The relative contributions of different peaks to the distribution of sputtered atoms are sensitive to the various parameters and especially to the interaction potential.²³ Therefore it is essential that the most realistic parameters as possible are used to get information about what really occurs in the Cu target during 5-keV Ar bombardment.

The geometries employed in the simulations are the same as in I (see Fig. 1). The 5-keV Ar projectile ions are incident along the z direction and impinge in a random position on the Cu(100) surface at normal incidence. $\theta = 0^\circ$ corresponds to the inward surface normal and $\theta = 180^\circ$ to the outward normal. The resulting cascades from 5000 projectile ions are followed, and when a recoil passes through a marker its direction and momentum vectors are logged. Since the collision chains

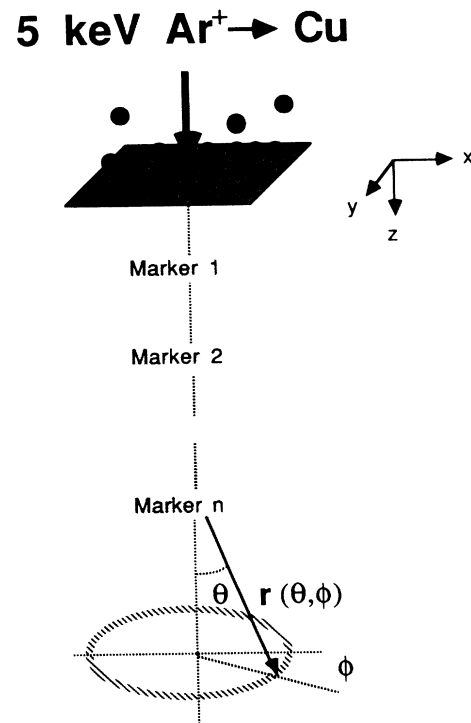


FIG. 1. Schematic illustration of the geometry used in the simulations.

may be long, the cascade termination was not used as in Ref. 18. The marker planes have no thickness and are parallel to the surface. The locations of the marker planes are indicated in the figure captions. The backup of the projectile is omitted when it is checked whether the recoil has passed a marker or not. After this check the backup is taken into account in the trajectory of the projectile. Thus, the asymptotical trajectories are calculated correctly. From the resulting angular distributions of recoils crossing marker planes, the recoil vector flux $N_r^m(\theta, \phi, z, E)$ is calculated. Because this flux N_r^m is not only contributed by the mass flow but also by the collision sequences transferring only energy, we call it modified recoil vector flux. Thus, if there is a collision sequence it is treated like a recoil with the same energy. The hypothetical distribution of sputtered particles at a depth z can be directly calculated from the modified recoil vector flux N_r^m as presented in paper I. One main modification compared to paper I is the inclusion of energy resolution in the recoil flux distributions. The whole energy range from the threshold energy $E_c=3.5$ eV to the primary energy $E_0=5$ keV is divided into intervals $(E_0/2^{n+1}, E_0/2^n)$, $n=0,1,2,\dots,10$. When a recoil crosses a marker, a check is made regarding the interval into which its energy falls.

The cascades are also parametrized by a parameter $f(z)$, which is calculated from the recoil direction vectors $\mathbf{r}(\theta, \phi)$. It represents the normalized net flow of recoils crossing a marker plane at depth z ,

$$f(z) = \frac{J_+ - J_-}{J_+ + J_-}, \quad (1)$$

where J_+ and J_- are the currents of recoils crossing the plane in question in the direction of the incident ion and towards the surface, respectively.¹⁹

B. Modeling the collision chains

The present version of COSIPO records different types of collision sequences and facilitates the extraction of detailed information about the contributions of collision chains propagating along definite atomic rows to vector fluxes and sputtering. We have mainly concentrated on chains that occur in the $\langle 100 \rangle$, $\langle 110 \rangle$, $\langle 111 \rangle$, and $\langle 112 \rangle$ directions because these are the most important rows in the case of fcc crystals. We have treated the following types of collision sequences separately.

(1) *Replacement chains.* The projectile replaces the next row atom on its lattice site if the projectile is left with a kinetic energy less than E_c and if it is closer to the target site than to its own original lattice site.

(2) *Focused chains.* In a focused collision sequence the knocked-out atom momentum is focused, which means that each particle moves at a smaller angle with the row than its predecessor. Assisted focusing,²⁹ in which the focusing action comes from rings of atoms surrounding the path of the sequence, is taken into account in the procedure and was not distinguished from Silsbee focusing,⁹

in which the focused chains occur along atomic rows that are isolated from their neighbors.

(3) *Defocused chains.* A defocused sequence is the opposite case to a focused one. The successive angles increase and the chain defocuses.

(4) *Directional collision chains.* In identifying directional collision chains, only the momentum transfer along an atomic row is taken into account, focusing being disregarded. Directional sequences can be focused, defocused, or mixed focused-defocused chains. These sequences always end in a focused or defocused chain.

Each type of collision sequence is also characterized by its length L . This parameter is defined in the following way. When a collision sequence, such as a replacement chain, is created the first atom in the sequence gets the label $i=0$. This atom replaces the next row atom on its lattice site and this atom is labeled $i=1$, which means that the length of the replacement chain is $L = t_{uvw}$ (t_{uvw} is the unit translation along an axis $[uvw]$) at that moment. If there is a marker plane between the first and second row atom, the first atom passes through the marker, but the replacement chain is not registered because at that moment it is not yet known whether the first atom replaces the next atom or not; in other words the replacement chain has not yet been created. Thus, the first atom is excluded in the procedure. Shulga¹³ has also used the same definition of collision sequences in connection with sputtering. The second atom with label $i=1$ may or may not replace the next row atom. If there is a marker between the second and the third row atom, the second atom passes through the marker and the replacement sequence is registered with length $L = t_{uvw}$. The replacement sequence is followed until it ends. Those events where the same projectile has traveled a longer distance than t_{uvw} and then replaces a row atom are not considered as replacement chains. The other types of collision sequences are recorded in an analogous way.

The program allows considerable flexibility in studying the role of each collision chain mechanism. One can omit certain type(s) of chains in the flux distributions either by terminating the chain when it is generated or simply leaving the chain out when it is found to cross the marker. Alternatively, one may record only a certain type of chain when it crosses a marker. Accordingly, we made several different calculations on which the discussion will be based: the whole cascade is calculated, certain type(s) of chains are truncated, and the whole cascade is calculated, but only certain type(s) of chains are recorded when crossing a marker. In practice only one type of chain was omitted or included, or all chains were omitted or included.

III. GENERAL FEATURES OF THE CASCADES

We first discuss some general features of a *statistical* cascade. Figure 2(a) shows the depth distribution of Ar ions and of both the nuclear and electronic energy losses of Ar ions. The projected range of the 5-keV Ar ions

in Cu(100) is $R_p \approx 100 \text{ \AA}$ and the depth distribution of the ions is peaked at about 20 \AA . Both of the distributions of energy losses have a maximum at the surface. The exceptional behavior of the nuclear energy loss is due to the structure of the target. The primary ion has the greatest possibility of losing its energy to the two first atomic layers; otherwise it has a large probability of being channelled. The contribution of electronic losses in total energy losses is a little over 10%, and it stays practically constant as a function of depth. Figure 2(b) presents the normalized currents $J(z)$, $J_+(z)$, and $J_-(z)$ when the markers are situated at symmetrical positions between two crystal planes. The currents are normalized to the sum of $J(z)$ over all marker depths z that

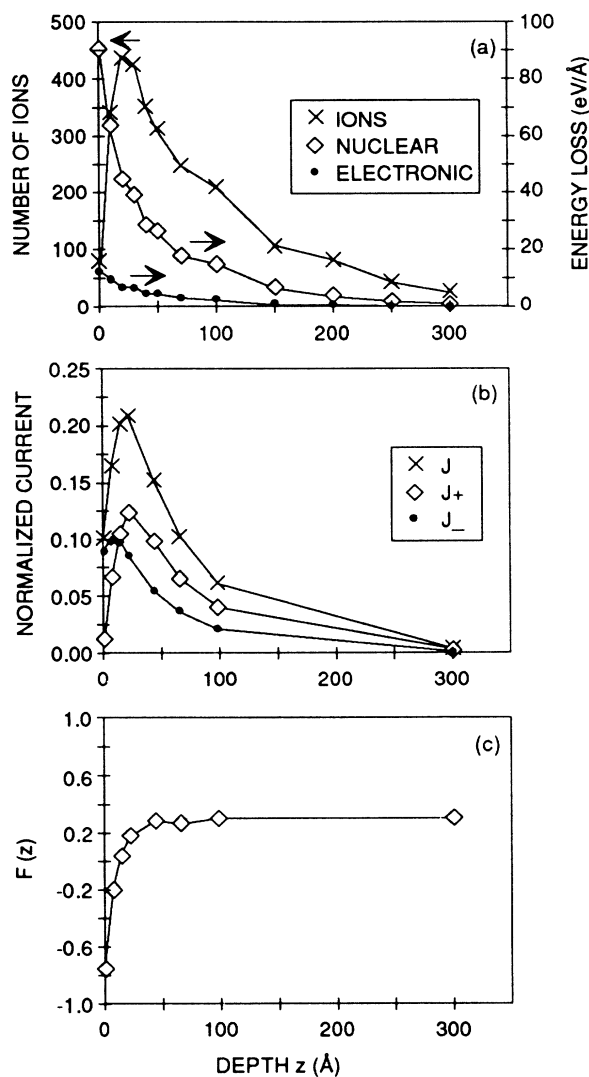


FIG. 2. (a) Depth distribution for 5-keV Ar ions slowing down in fcc Cu (\times) and depth distributions of nuclear (\diamond) and electronic (\bullet) energy loss of the primary ions. (b) Total current $J(z)$ of recoils (\times), currents J_+ (\diamond) and J_- (\bullet) in the direction of the incoming ion and towards the surface. (c) Parameter $f(z)$ as a function of depth z . The markers are situated symmetrically between two crystal planes.

have been considered.¹⁹ The total current $J(z)$ and the depth distribution of the incoming ions have maxima at equal depths. The distribution of total current J agrees with that of created vacancies (not shown). Although the damage is a consequence of the transfer of energy from the primary ion to the target atoms, the damage profile cannot be obtained directly from the calculation of the nuclear energy loss of the incoming ion. This is due to the fact that the energy transport by recoils is never negligible especially near the surface and also due to the fact that the recoils lose their energy to electrons. From Fig. 2(b) it can be observed that the maximum of $J(z)$ is due to recoils moving in the forward direction, i.e., due to J_+ . The J_- distribution is peaked at a little over 10 \AA . The position of the maximum corresponds to the depth where the parameter $f(z)$ is close to zero [see Fig. 2(c)]. Near the surface the recoils are backward-directed [$f(z) < 0$]. This near-surface backward directed recoil flux is associated with low-energy recoils. Deeper in the target recoils have a forward direction [$f(z) > 0$]. This same behavior was also reported in our earlier paper.¹⁹

IV. DEPTH DEPENDENCE OF THE COLLISION CASCADE

The evolution of the anisotropies of a statistical cascade will be studied as a function of the depth of the marker by using the modified recoil vector flux distributions N_r^m , which bear a resemblance to the distribution of sputtered particles. In the following the markers are always situated in the middle of the crystal planes as in paper I. This selection of the marker position has already been discussed in paper I. In addition to depth dependence, the significance of various collision chain mechanisms will be studied in connection with the spots observed in the flux distributions.

The dependence of a statistical cascade as a function of distance from the target surface is given in Fig. 3. A Cu(100) surface is bombarded with 5-keV Ar ions at normal incidence. The marker plane is situated at depths $z=0.9, 8.1, \text{ and } 18.9 \text{ \AA}$. This selection of the marker positions is sufficient to show the most important features of the evolution of the anisotropies. Figure 3(a) shows the modified recoil vector flux distribution N_r^m in the backward direction at depth $z=0.9 \text{ \AA}$. In the figure only the azimuthal angles $0^\circ < \phi < 90^\circ$ are shown because of the symmetry. The distribution is dominated by the $\langle 110 \rangle$ peaks ($\theta = 135^\circ, \phi = 0^\circ, 90^\circ$). In addition to these peaks, one can observe smaller $\langle 100 \rangle$ ($\theta = 180^\circ, \phi$ is arbitrary) and $\langle 111 \rangle$ ($\theta = 125^\circ, \phi = 45^\circ$) peaks. The faint band between the $\langle 110 \rangle$ peaks is mainly due to replacement and defocused chains. In the backward direction the N_r^m distribution is dominated by these peaks still at depths of the order of 200 \AA , and the distribution stays practically similar to that in Fig. 3(a).

Figures 3(b)–3(d) present the N_r^m distribution in the forward direction at depths $z=0.9, 8.1, \text{ and } 18.9 \text{ \AA}$. The distribution in the forward direction in Fig. 3(b) is dom-

inated by a band with $45^\circ \leq \theta \leq 65^\circ$. These recoils have mostly low energies ($E < 20$ eV), which means that they cannot be primary knock-on atoms (PKA). Scattering kinematics limit low-energy primary recoils ($E < 20$ eV) to the angular range $\theta > 85^\circ$. Thus, the recoils in the band in Fig. 3(b) are due to more complicated collision mechanisms. The mechanisms leading to this band will be discussed in connection with Fig. 4. In addition to the band in Fig. 3(b) there is a small peak at $\theta \approx 60^\circ$, $\phi \approx 45^\circ$. The origin of this peak will be studied in connection with Fig. 4(c). One can observe a step at $\theta \approx 110^\circ$ in Fig. 3(a) and $\theta \approx 70^\circ$ in Figs. 3(b)–3(d). This is due to scattering kinematics, and the exact value of the polar angle θ depends on the position of the marker with respect to the crystal plane below the marker. An

approximate value for θ can be calculated by insisting that the deflection point (without backup) of the trajectory of a recoil lies on the marker. The recoils have originated from an atomic plane just below or above the marker plane. In our case a simple trigonometrical calculation gives 67.5° for θ , which corresponds well to the position of the step in Fig. 3. At higher polar angles it is mainly channelled recoils that cross the marker.

When the depth of the marker increases, the band is the dominating structure up to $z \approx 6.3$ Å in the N_r^m distribution in the forward direction, i.e., until the $\langle 110 \rangle$ peaks start to develop. In Fig. 3(c) ($z=8.1$ Å) these peaks are pronounced as well as in Fig. 3(d) ($z=18.9$ Å). In addition to these peaks there are also $\langle 100 \rangle$ ($\theta = 0^\circ$) and small $\langle 111 \rangle$ ($\theta = 55^\circ$) peaks. Calculations show that

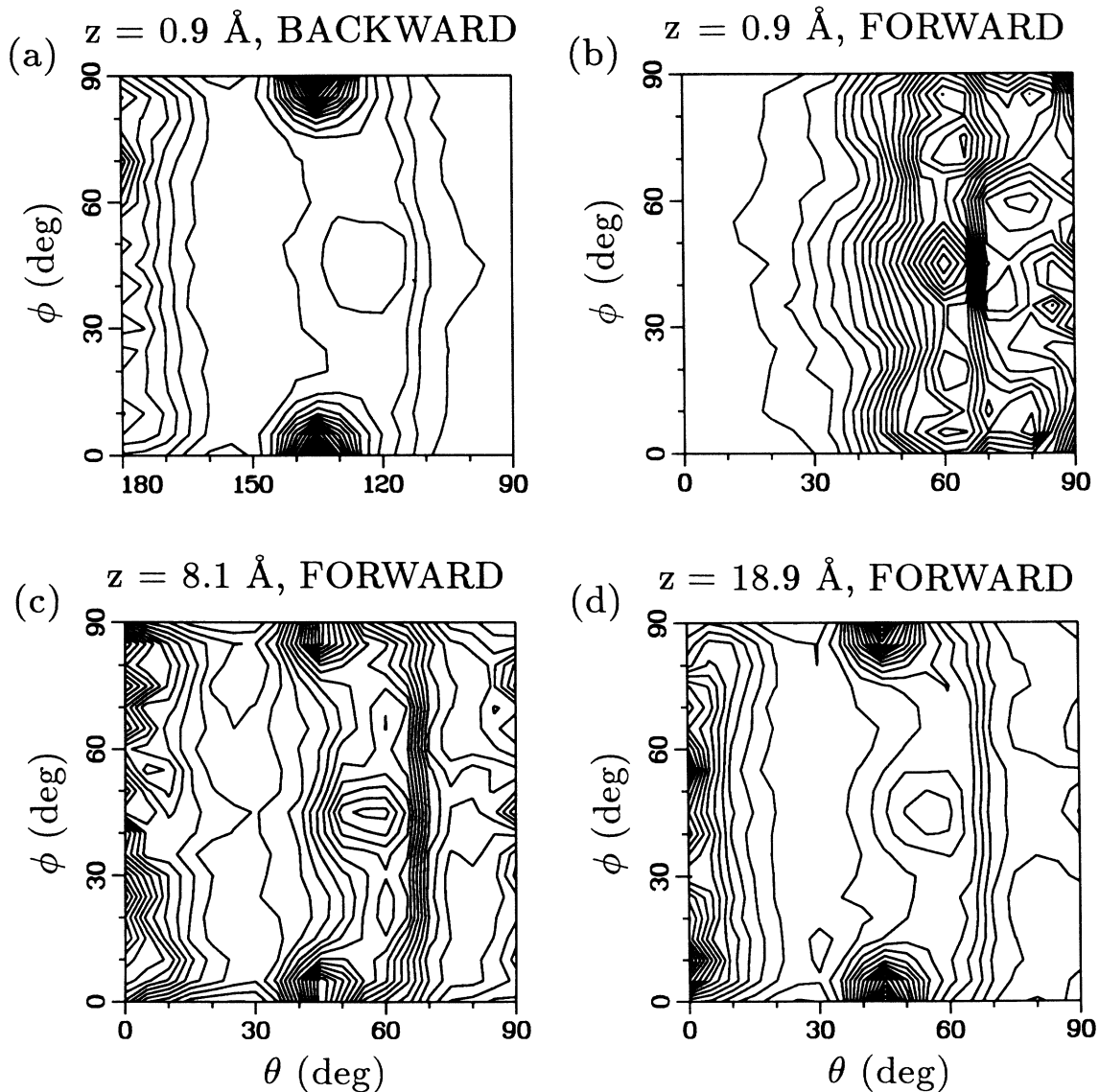


FIG. 3. Modified recoil vector flux distributions $N_r^m(\theta, \phi, z)$. The markers are situated symmetrically between two atomic planes at depths $z=0.9$ Å (a) and (b), 8.1 Å (c), and 18.9 Å (d). The distribution is for backward-directed recoils in (a) and for forward-directed recoils in (b)–(d).

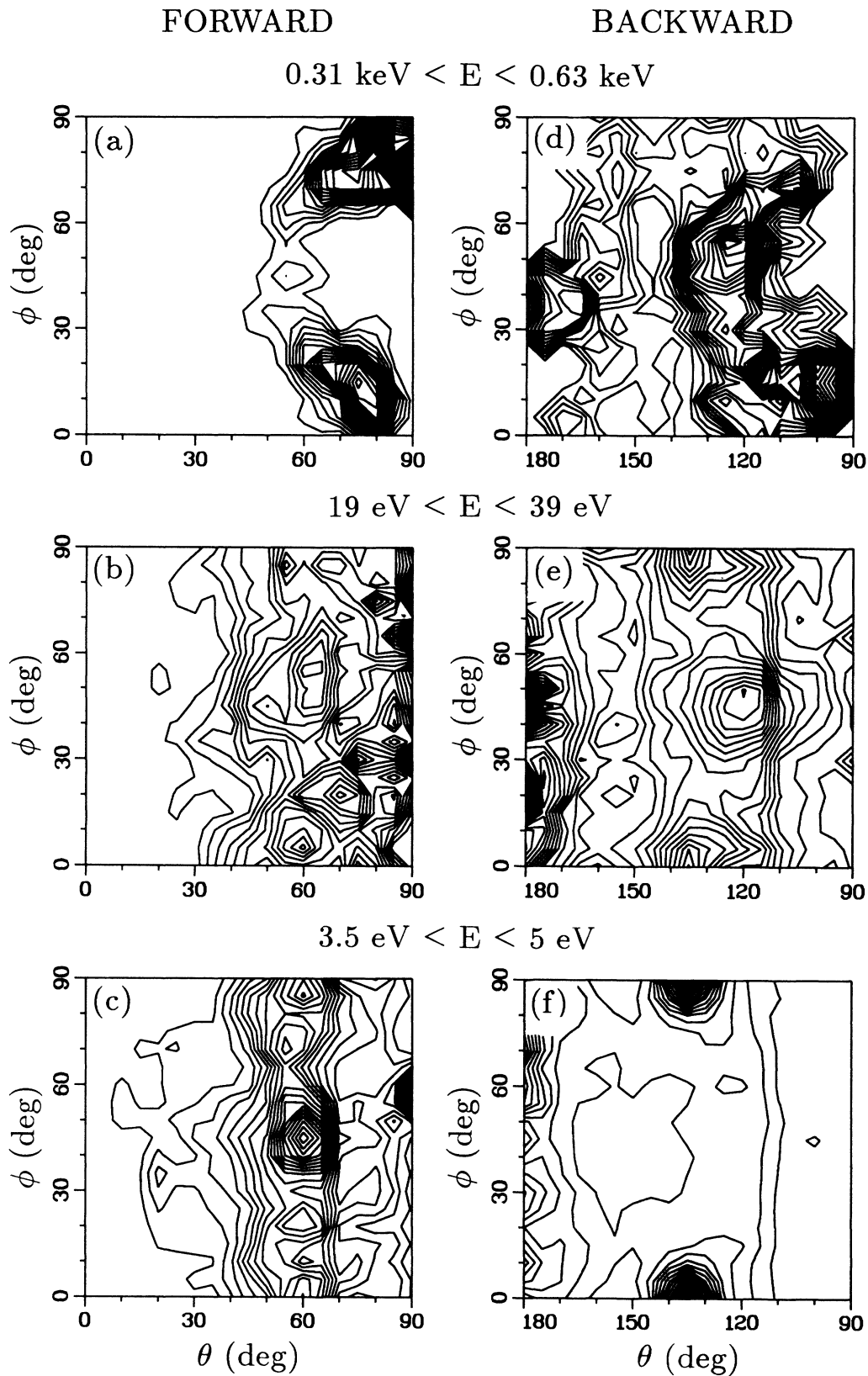


FIG. 4. Modified recoil vector flux distributions $N_r^m(\theta, \phi, E)$ as a function of energy. The marker is at the depth $z=0.9 \text{ \AA}$. The energy intervals of the recoils are $0.31 \text{ keV} < E < 0.63 \text{ keV}$ (a) and (d), $19 \text{ eV} < E < 39 \text{ eV}$ (b) and (e), $3.5 \text{ eV} < E < 5 \text{ eV}$ (c) and (f). The recoils are forward directed in (a)–(c) and backward directed in (d)–(f).

the modified recoil flux is dominated by the $\langle 110 \rangle$ peaks in both directions at symmetrical marker positions even when the depth of the marker is of the order of twice the projected range of the incoming ion ($R_p \approx 100 \text{ \AA}$).

V. ENERGY DEPENDENCE OF THE CASCADE

Figure 4 shows the N_r^m distributions and the development of collision cascade anisotropies as a function of energy when the marker is at the depth $z=0.9 \text{ \AA}$ and the energy is less than 0.63 keV . In Figs. 4(a)–4(c) the recoils are forwardly directed and in Figs. 4(d)–4(f) backward directed, respectively. The recoils with energies over 0.63 keV are mainly PKA's with a definite energy. Therefore the N_r^m distributions with intervals of higher energy (not shown) are formed by a band: a definite polar angular region with the azimuthal angle being random. In Fig. 4(a) ($0.31 \text{ keV} < E < 0.63 \text{ keV}$) the peaks ($\theta \approx 80^\circ$, $\phi \approx 15^\circ, 75^\circ$) are due to several collision mechanisms. If the impact parameter is not too small, the recoil energy is low and the recoil is directed to an angle near 90° . In most cases the impact point of the ion is close to $\langle 100 \rangle$ rows and the recoil in the surface is directed approximately in the $\langle 100 \rangle$ direction. After one or several collisions it passes through the marker. If the ion impact is close to the $\langle 110 \rangle$ row, the recoil may collide with the next $\langle 110 \rangle$ row atom before crossing the marker. This is why the angular region near $\phi = 45^\circ$ is missing from the band. In Fig. 4(b) ($19 \text{ eV} < E < 39 \text{ eV}$) the recoils are moving almost in the direction of the marker. Some of them are PKA's ($\theta > 85^\circ$), while others are due to more complicated collision mechanisms. These mechanisms are mainly $\langle 100 \rangle$ and $\langle 110 \rangle$ collision sequences propagating originally along the surface. When the energy dissipates further, the distributions have a band with $45^\circ < \theta < 65^\circ$.

The recoils belonging to the band in Fig. 4(c) ($3.5 \text{ eV} < E < 5 \text{ eV}$) and the recoils with somewhat higher energies ($5 \text{ eV} < E < 20 \text{ eV}$) and with polar angles in the range $45^\circ < \theta < 65^\circ$ dominate the N_r^m distribution in Fig. 3(b). We can divide the mechanisms leading to the band roughly into two groups. The point of impact of the incoming ion is close to the $\langle 100 \rangle$ or $\langle 110 \rangle$ rows and the target atom in the surface is directed in either one of these directions. After one or several collisions the momentum is directed into the crystal. The second collision mechanism is more complicated because it is based on momentum reversal, which occurs at the second atom layer or deeper in the target. A collision chain is initiated towards the surface. At the surface the momentum is again directed into the target. These mechanisms are basically the same as those studied in Ref. 30 in connection with sputtering. The peak in Fig. 4(c) at $\theta \approx 60^\circ$ and $\phi \approx 45^\circ$ is mainly due to $\langle 110 \rangle$ collision sequences originally propagating along the surface. At some stage the momentum is turned into the crystal. The same peak was also observed in Fig. 3(b).

In the backward direction the N_r^m distributions are more or less structureless when the recoil energy is hundreds of eV [Fig. 4(d), $0.31 \text{ keV} < E < 0.63 \text{ keV}$]. Definite conclusions about collision mechanisms cannot be made because statistics are quite poor at these energies. The $\langle 100 \rangle$ and $\langle 111 \rangle$ peaks emerge at the energy interval $0.16 \text{ keV} < E < 0.31 \text{ keV}$. The $\langle 110 \rangle$ peaks start to develop at lower energies and they can be observed in Fig. 4(e) ($19 \text{ eV} < E < 39 \text{ eV}$). The $\langle 110 \rangle$ spots become more pronounced when the energy gets smaller [Fig. 4(f), $3.5 \text{ eV} < E < 5 \text{ eV}$].

VI. COLLISION SEQUENCE MECHANISMS

A. Generation of the first recoil in a collision sequence

At low bombarding ion energies ($\lesssim 100 \text{ eV}$) it is possible to explain spot patterns of sputtered particles in terms of simple collision mechanisms. When higher bombarding energies ($\gtrsim 1 \text{ keV}$) are used it becomes more difficult to define individual processes. At low energies the ion penetrates a couple of monolayers and the mechanisms are tractable. When the energy is higher, the ion penetrates several monolayers and long collision sequences are possible. In this section the purpose is to discuss some qualitative aspects of the creation of collision sequences. No definite mechanisms leading to a certain type of collision chain are given here. The diversity of processes becomes evident when Fig. 5 is studied. It shows the fractions of different generations g of the first recoil in a replacement [Fig. 5(a)], focused [Fig. 5(b)], defocused [Fig. 5(c)], and directional [Fig. 5(d)] collision chain. If one collision mechanism were dominating when a sequence is initiated, the distribution would be strongly peaked at a definite generation. The marker is at a depth $z=0.9 \text{ \AA}$, and the recoils are moving in the backward direction. The generations $g \geq 11$ are omitted in the calculations. The total number of chains (with generations $g=1-10$) in a certain direction in all the figures is taken to be 100%.

The generation of the first recoil in a chain is mostly 2–4 irrespective of the direction and type of the sequence. This situation also prevails at other marker depths. As explained in Sec. II B, this first recoil initiating a sequence is not registered as a member of a chain when crossing a marker. The generation of the first recoil is quite independent of the length and type of the sequence. The fractions of higher generations ($g \geq 5$) decrease quite rapidly except in the cases of the $\langle 110 \rangle$ focused and defocused chains [Figs. 5(b)–5(c)]. The contribution of generation $g=10$ is about 4% in these cases. The lengths of the $\langle 110 \rangle$ focused and defocused chains with generations $g \geq 5$ of the first recoil are mostly $1-2t_{110}$ in Fig. 5(b) and t_{110} in Fig. 5(c). This shows clearly the diversity of processes leading to the $\langle 110 \rangle$ focused or defocused chains, i.e., usually the number of collisions needed to initiate a sequence is quite small, but the chain can also

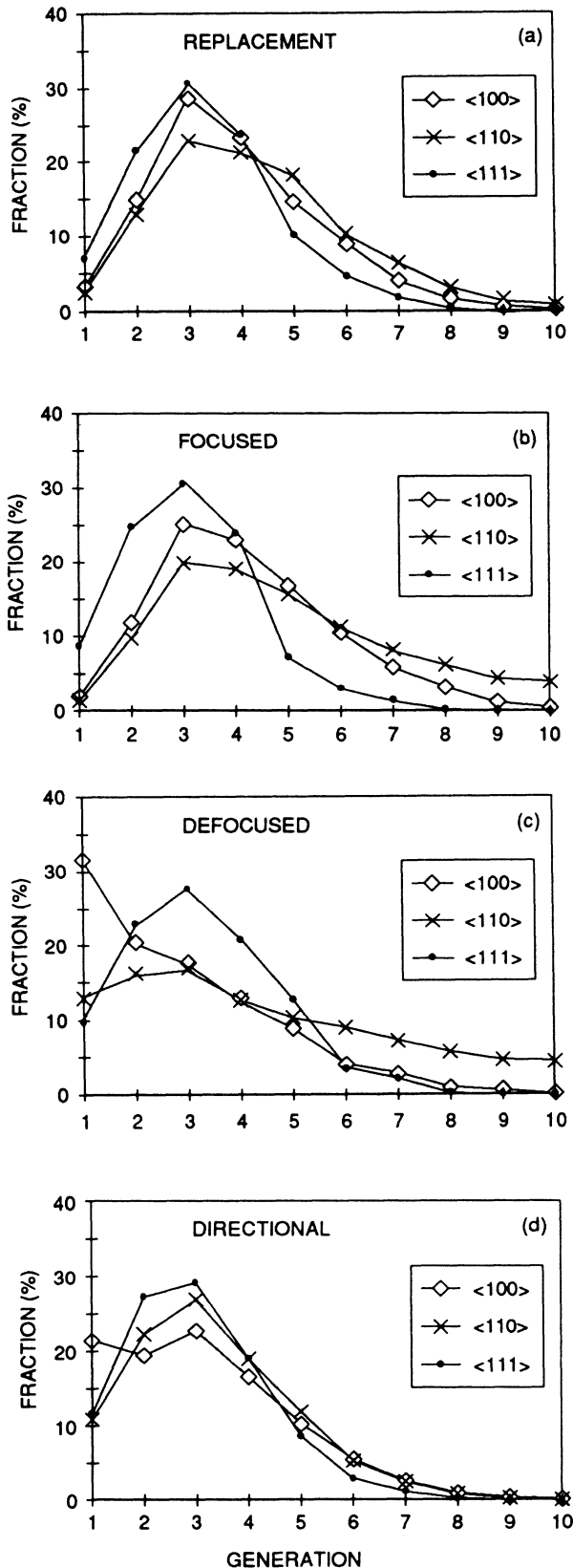


FIG. 5. Generation of the first recoil in a replacement (a), focused (b), defocused (c), and directional (d) chain. The marker is at the depth $z=0.9 \text{ \AA}$ and recoils move in the backward direction.

be created after several collisions. The generation $g=10$ makes a notable contribution, too. The high fraction of generations $g \geq 5$ is due to transitions from defocused to focused sequence and vice versa. In Figs. 5(c) and 5(d) the high contributions of generations $g=1$ in the case of the $\langle 100 \rangle$ direction is noteworthy. Deeper in the target this behavior is not observed. This is partly due to the fact that the generation $g=1$ is mainly connected to length $L = t_{uvw}$, and deeper in the target the contribution of length $L = t_{uvw}$ decreases relatively more than for other lengths. On the other hand, deeper in the target other collision mechanisms leading to the $\langle 100 \rangle$ defocused or directional chains (with higher generations of the first recoil) become more dominant. The distributions for the $\langle 111 \rangle$ direction are more peaked, and the contributions of generations $g \geq 5$ are lower than in other directions. This can be attributed to the fact that the recoils in the $\langle 111 \rangle$ direction are more energetic than the recoils in other directions and the $\langle 111 \rangle$ chains cannot be created at low energies after several collisions. At other marker depths in the backward direction generations 2–4 are also dominating and the distributions are qualitatively similar to those in Fig. 5. There are some minor exceptions, e.g., in Figs. 5(c)–5(d) the $\langle 100 \rangle$ chains.

In the forward direction and near the surface ($z \lesssim 10 \text{ \AA}$) the generation of the first recoil is mostly 1–3, i.e., the number of collisions needed to initiate a sequence is somewhat smaller than in the backward direction. Deeper in the target ($z \gtrsim 10 \text{ \AA}$) the distributions of generations are qualitatively quite similar to the corresponding ones in the backward direction, and they usually have a maximum at equal generations in both directions.

B. Contribution of collision sequences to the flux distributions

The contribution of different collision sequences to the modified recoil vector flux is shown in Fig. 6 as a function of length of the chain at the marker depth $z=0.9 \text{ \AA}$ in the backward direction. The length $L = 15t_{uvw}$ contains all chains of length $L \geq 15t_{uvw}$. The scale of the vertical axis (expressed as a percentage) is obtained by dividing the number of the collision chains by the number of recoils crossing the marker in the upward direction. The corresponding distributions in the forward direction are not shown because of large statistical fluctuations due to the rare occurrence of collision sequences near the surface. Deeper in the target the distributions are qualitatively quite similar to those in Fig. 6. Near the surface ($z \lesssim 10 \text{ \AA}$) the collision sequences are clearly shorter and the contribution of long-range chains lower in the forward direction than in the backward direction. At depths $z \gtrsim 15 \text{ \AA}$ the differences in the mean lengths have diminished markedly. However, at depths $z \gtrsim 15 \text{ \AA}$ the contributions of different chains to the vector flux are higher in the forward direction than in the backward direction. This is accounted for by the fact that the cascade is forward directed at depths $z \gtrsim 15 \text{ \AA}$.

Replacement sequences [see Fig. 6(a)] propagate most

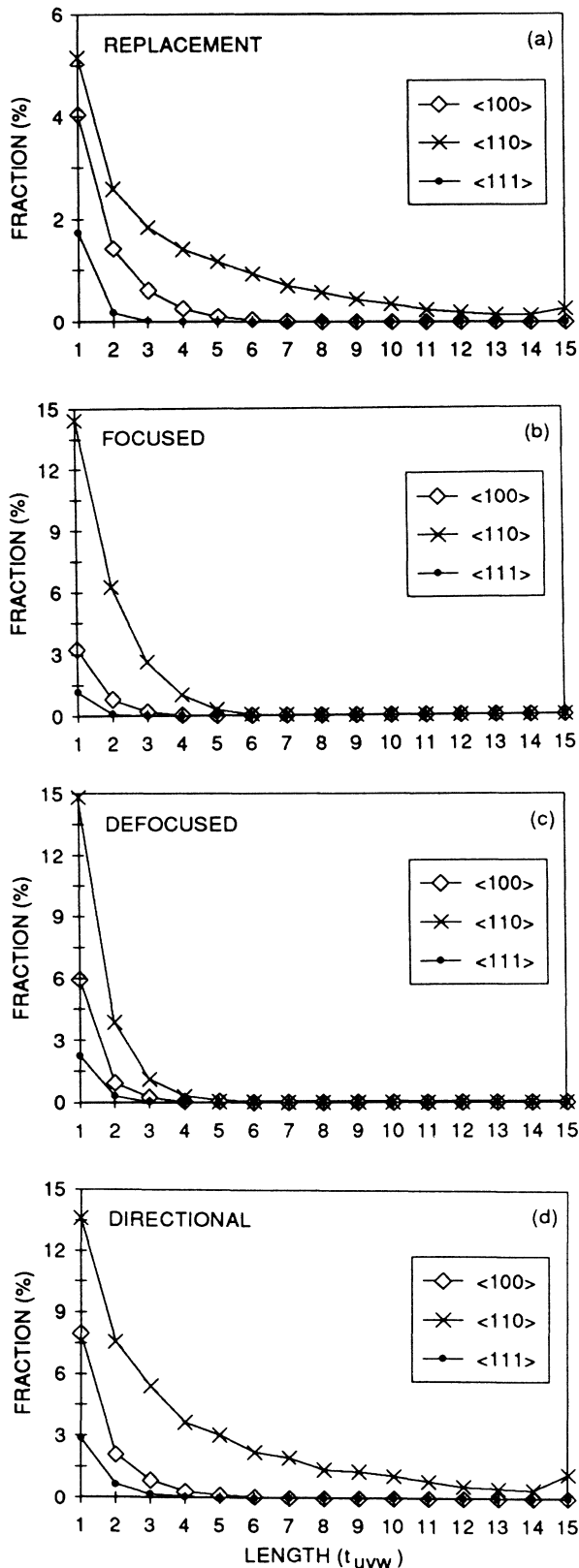


FIG. 6. Contribution of different collision sequences to the modified recoil vector flux in the backward direction. The marker is situated at the depth $z=0.9$ Å. Replacement sequences are presented in (a), focused in (b), and defocused in (c). The contribution of directional chains is shown in (d).

frequently along the $\langle 110 \rangle$ rows, though long-range chains ($L \geq 3t_{uvw}$) along these rows also have a notable role. The $\langle 111 \rangle$ replacement chains make the smallest contribution. The replacement sequences are mainly of the short-range type except the $\langle 110 \rangle$ chains (see Table I). This behavior is to be expected because the $\langle 110 \rangle$ direction has the closest packing and the least energy loss to focusing rings, while for the $\langle 111 \rangle$ direction the situation is exactly the opposite. This also holds for other types of collision chains. In addition to this, the least energy needed to overcome the midpoint between two lattice sites of a row [called replacement energy E_r (Ref. 31)] is lowest for the $\langle 110 \rangle$ direction, while highest for the $\langle 111 \rangle$ direction. The fractions of the replacement sequences of all lengths in the backward direction are shown in Table II. When the $\langle 112 \rangle$ chains are included, the total contribution of replacement sequences to the flux is 27% in the backward direction at the marker depth $z=0.9$ Å. The contribution of replacement sequences can also be studied by truncating them in the cascades in a similar way as in Ref. 12. In this type of calculation, replacement sequences are truncated, which means that when a recoil is going to replace the next row atom on its lattice site the program does not include this collision, ignores the recoil, and begins to follow a completely different recoil. The contributions of replacement sequences are obtained by subtracting the flux distributions from the distributions calculated in the normal way and by dividing the differences by the normal distributions. The flux distributions remain, however, strongly anisotropic even though the $\langle 110 \rangle$ peaks have become smaller. The fraction of replacement sequences in the flux distributions in the backward direction calculated by terminating them becomes too high (55%) compared to normal calculations. The truncation of replacement sequences does not give correct contributions because the whole cascade is not calculated. It gives, however, some indications of anisotropies in collision cascades.

When Figs. 6(a) and 6(b) are compared to each other, one can observe that the role of the focused sequences is more pronounced than that of the replacement chains, but the focused sequences are clearly of a shorter-range type than the replacement ones. The $\langle 110 \rangle$ focused sequences are the most dominant and the $\langle 111 \rangle$ chains make the least contribution, as is the situation with other types of collision sequences. The mean lengths of the $\langle 100 \rangle$ and the $\langle 111 \rangle$ focused chains are only a little smaller than the corresponding lengths of the replacement sequences, though the $\langle 110 \rangle$ focused chains are much shorter than the $\langle 110 \rangle$ replacement ones (see Table I). The fractions of focused sequences of all lengths in the modified vector flux in the backward direction are shown in Table II.

The defocused chains [Fig. 6(c)] play a somewhat more important role than the focused chains. The defocused sequences are distinctly of the short-range type and have somewhat smaller mean lengths than the focused ones except in the case of the $\langle 111 \rangle$ direction (see Table I). The differences between the mean lengths of the focused

TABLE I. The mean lengths of the $\langle 100 \rangle$, $\langle 110 \rangle$, and $\langle 111 \rangle$ collision sequences. The unit is t_{uvw} (the unit translation along an axis $[uvw]$). The marker is at the depth $z=0.9 \text{ \AA}$. Recoils move in the backward direction. The statistical uncertainty is less than $0.05 t_{uvw}$. The unit translation along the axes are $t_{100}=3.61 \text{ \AA}$, $t_{110}=2.55 \text{ \AA}$, and $t_{111}=6.25 \text{ \AA}$.

Chain	Replacement	Focused	Defocused	Directional
$\langle 100 \rangle$	1.66	1.31	1.23	1.51
$\langle 110 \rangle$	3.93	1.65	1.36	4.13
$\langle 111 \rangle$	1.12	1.08	1.15	1.34

or defocused sequences in different directions are not so pronounced as in the case of the replacement chains. In the case of focused chains this is due to thermal vibrations that attenuate them efficiently. The effect of thermal vibrations will be discussed later. Defocused sequences are mainly of the short-range type irrespective of temperature. When the contributions of defocused chains of all lengths to the modified vector flux in the backward direction are compared to the corresponding numbers of the focused sequences, one observes that in the $\langle 110 \rangle$ direction the focused sequences are somewhat more dominant than the defocused ones (see Table II). The situation is contrary to the $\langle 100 \rangle$ and the $\langle 111 \rangle$ directions. This shows that focusing along $\langle 110 \rangle$ directions is very efficient. The fraction of the defocused chains in the modified vector flux in the backward direction is somewhat higher than that of the focused chains. This is accounted for by thermal vibrations, which hamper a focused transfer of momentum efficiently. When thermal vibrations are omitted, the focused sequences make a higher contribution to the modified vector flux than the defocused ones.

The directional collision sequences [Fig. 6(d)] can be focused, defocused, or mixed. This means that $F_{(uvw)} + C_{(uvw)} = D_{(uvw)}$ for a certain marker if the contributions from the collision sequences of all lengths are summed up. F stands for focused, C for defocused, and D for directional sequence, respectively. This is accounted for by the fact that each directional collision sequence always ends in a focused or defocused chain. However, this equality is violated for chains of a definite length, since focused, defocused, and directional chains are distributed over their lengths differently. This can be observed when Figs. 6(b)–6(d) are compared to each other. The $\langle 110 \rangle$ and $\langle 111 \rangle$ directional chains are somewhat longer than the corresponding replacement ones, though the $\langle 100 \rangle$ directional sequences are shorter than

the $\langle 100 \rangle$ replacement ones (see Table I). The fractions of directional chains of all lengths in the modified recoil flux in the backward direction can be obtained by summing the corresponding contributions of the focused and defocused chains (see Table II).

When the marker is at the depth $z=15.3 \text{ \AA}$ the contributions of collision sequences are qualitatively quite similar to the corresponding ones for when the marker is near the surface [Figs. 6(a)–6(d)]. Tables III and IV present the mean lengths and the fractions of the $\langle 100 \rangle$, $\langle 110 \rangle$, and $\langle 111 \rangle$ collision sequences directed in the backward direction. The replacement and directional collision chains are of a longer-range type than the focused and defocused ones. The differences between the mean lengths at various marker positions are usually quite small in the backward direction except in the case of the $\langle 110 \rangle$ replacement and directional chains. The changes in the mean lengths are not wholly systematic. One would expect that the mean lengths are higher near the surface than deeper in the target in the case of the backward direction. This is the situation in most cases, but there are some exceptions. In the forward direction the mean lengths usually increase as a function of depth. The chains do not, however, necessarily terminate when passing through a marker. At the depth $z=15.3 \text{ \AA}$ the mean lengths in the forward direction are only a little smaller than in the backward direction except in the cases of $\langle 110 \rangle$ replacement and directional collision sequences for which the differences are pronounced. This is quite natural, since the collision chains are mostly of the short-range type (except the $\langle 110 \rangle$ replacement and directional ones) and are almost fully developed in both directions, whereas the $\langle 110 \rangle$ replacement and directional sequences are of the longer-range type and are not fully developed in either direction. The contributions of the $\langle 100 \rangle$, $\langle 110 \rangle$ and $\langle 111 \rangle$ collision sequences (in the backward direction) to the modified recoil flux at the depth $z=15.3 \text{ \AA}$ are some-

TABLE II. The contributions of $\langle 100 \rangle$, $\langle 110 \rangle$, and $\langle 111 \rangle$ collision sequences of all lengths to the modified recoil vector flux in the backward direction. The marker is at the depth $z=0.9 \text{ \AA}$. The total contains all chains of the certain type. The statistical uncertainty is less than 5%.

Chain	Replacement (%)	Focused (%)	Defocused (%)	Directional (%)
$\langle 100 \rangle$	6.5	4	7	12
$\langle 110 \rangle$	16	25	20	45
$\langle 111 \rangle$	2	1	3	4
Total	27	31	38	69

TABLE III. The mean lengths of the $\langle 100 \rangle$, $\langle 110 \rangle$, and $\langle 111 \rangle$ collision sequences. The unit is t_{uvw} (the unit translation along an axis $[uvw]$). The marker is at the depth $z=15.3$ Å. Recoils move in the backward direction. The statistical uncertainty is less than $0.04 t_{uvw}$.

Chain	Replacement	Focused	Defocused	Directional
$\langle 100 \rangle$	1.55	1.27	1.24	1.44
$\langle 110 \rangle$	3.35	1.59	1.36	3.51
$\langle 111 \rangle$	1.14	1.06	1.09	1.25

what lower than at the depth $z=0.9$ Å. In the forward direction and at the depth $z=15.3$ Å the fractions of the chains as a function of length (not shown) are quite similar to those in the backward direction. Note that at this depth the parameter $f(z)$ is close to zero [see Fig. 2(c)].

C. Contribution of chains to the $\langle 100 \rangle$, $\langle 110 \rangle$, and $\langle 111 \rangle$ peaks at different depths

The effect of different collision chain mechanisms on the $\langle 100 \rangle$ and $\langle 110 \rangle$ peaks is shown in Fig. 7 for various marker positions. The $\langle 110 \rangle$ spot is limited by angles $\theta = 32.5^\circ$ – 57.5° ($\theta = 122.5^\circ$ – 147.5°) and $\phi = -12.5^\circ$ – 12.5° in the forward (backward) direction and the $\langle 100 \rangle$ peak by angles $\theta = 0^\circ$ – 12.5° ($\theta = 167.5^\circ$ – 180°) in the forward (backward) direction, correspondingly. The fractions (in percentages) of various collision chains in the $\langle 100 \rangle$ and $\langle 110 \rangle$ peaks have been calculated by dividing the number of the corresponding sequence by the number of all recoils in the peak. It must be pointed out that the distributions in Figs. 6 and 7 have a different meaning. Figure 6 presents the contribution of various collision sequences to the modified vector flux, whereas Fig. 7 shows the contribution to the $\langle 100 \rangle$ and $\langle 110 \rangle$ peaks. Figures 7(a)–7(d) show the contributions of replacement, focused, directional, and all collision sequences to the $\langle 110 \rangle$ peaks and 7(e)–7(h) to the $\langle 100 \rangle$ peaks, respectively. In the forward direction the fractions are presented beginning from the depth $z=4.5$ Å because of large statistical fluctuations nearer the surface. In the backward direction the contribution of various collision-chain mechanisms to the $\langle 110 \rangle$ and $\langle 100 \rangle$ peaks either decreases only slightly as a function of depth or stays almost constant. The development of the cascade can be observed in the forward direction as the role of the collision chains becomes more important when the distance of the marker plane from the surface increases. In the case of the $\langle 110 \rangle$ peaks the contribution of replacement [Fig. 7(a)] and focused [Fig. 7(b)] sequences is the most significant in both di-

rections. Defocused chains (not shown) make a smaller contribution to the $\langle 110 \rangle$ peaks. When Figs. 7(a)–7(d) are compared to each other one can observe that at the marker depths $z=11.7$ and 15.3 Å the fractions of collision sequences in both directions are almost similar. This is the depth where the parameter $f(z)$ is close to zero, which means that the numbers of recoils going upwards and downwards are almost equal [see Fig. 2(c)]. Deeper in the target the contributions of distinct sequences are practically equal in both directions and a slight increase in them in the forward direction can be noticed as a function of depth.

The depth dependence of the contribution of the collision sequences to the $\langle 100 \rangle$ peak is analogous to the case of the $\langle 110 \rangle$ peaks. From Fig. 7 it can be seen that the role of different collision sequences to the $\langle 100 \rangle$ peak is somewhat less significant than to the $\langle 110 \rangle$ peaks. In addition to this, the increase in the fraction of different chains in the $\langle 100 \rangle$ peak occurs deeper in the target than in the case of the $\langle 110 \rangle$ peaks and it has not been levelled down in the forward direction in the case of the $\langle 100 \rangle$ peaks. This shows very clearly that the $\langle 110 \rangle$ chains are more stable than the $\langle 100 \rangle$ ones. Deeper in the target ($z \approx 18$ Å) the contributions of the chains are practically equal in both directions. Replacement and defocused chains play the most important role in the case of the $\langle 100 \rangle$ peak. Overall, we may conclude that the linear collision sequences are the principal mechanism behind the $\langle 100 \rangle$ and the $\langle 110 \rangle$ peaks. The contribution of all collision chains to the $\langle 110 \rangle$ peaks is 91% and to the $\langle 100 \rangle$ peak 67% on average in the backward direction (see Table V).

In the case of the $\langle 111 \rangle$ peak the fractions of replacement, focused, and all chains in the $\langle 111 \rangle$ peaks are on average 15, 10, and 50 % in the backward direction. Thus the role of the collision sequences to the $\langle 111 \rangle$ peak is not so pronounced as in the case of the $\langle 100 \rangle$ and the $\langle 110 \rangle$ peaks. The part in these peaks that is not due to collision sequences can be attributed to low-energy

TABLE IV. The contributions of $\langle 100 \rangle$, $\langle 110 \rangle$, and $\langle 111 \rangle$ collision sequences of all lengths to the modified recoil vector flux in the backward direction. The marker is at the depth $z=15.3$ Å. The total contains all chains of the certain type. The statistical uncertainty is less than 5%.

Chain	Replacement (%)	Focused (%)	Defocused (%)	Directional (%)
$\langle 100 \rangle$	5	3	6	9
$\langle 110 \rangle$	15	23	20	43
$\langle 111 \rangle$	2	1	2	3
Total	25	29	36	65

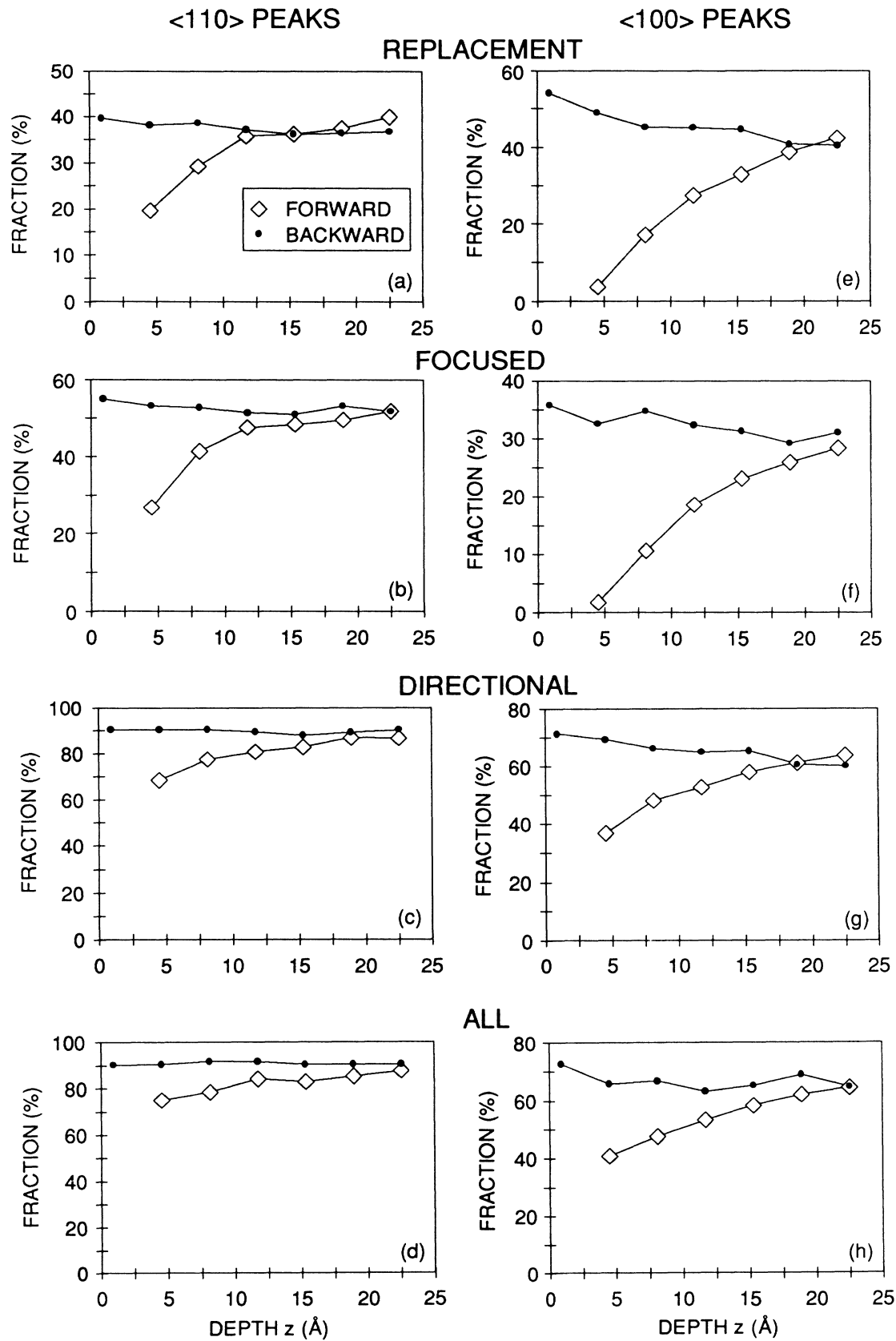


FIG. 7. Contribution of distinct collision sequences to the $\langle 110 \rangle$ peaks (a)–(d) and to the $\langle 100 \rangle$ peaks (e)–(h). Replacement sequences are presented in (a) and (e), focused in (b) and (f), directional chains in (c) and (g). The contribution of all collision chains is shown in (d) and (h).

TABLE V. The average contributions of the $\langle 100 \rangle$, $\langle 110 \rangle$, and $\langle 111 \rangle$ collision sequences of all lengths to the $\langle 100 \rangle$ and $\langle 110 \rangle$ peaks in the modified recoil flux in the backward direction.

Direction	$\langle 100 \rangle$ peak (%)	$\langle 110 \rangle$ peak (%)
$\langle 100 \rangle$	44	2
$\langle 110 \rangle$	6	82
$\langle 111 \rangle$	1	1
All	67	91

channeling and “random” background in these low-index directions. When all the collision sequences are omitted in the flux distributions, although the whole cascade is calculated, the $\langle 110 \rangle$ peaks disappear and the distributions are dominated by the $\langle 100 \rangle$ and $\langle 111 \rangle$ peaks in both directions. Some calculations were made to resolve the contribution of channeling. A recoil is regarded as channelled if it has traveled a longer distance than t_{uvw} along the direction $[uvw]$. In the case of the $\langle 100 \rangle$ peak the fraction of channeling is about 13% on average in the backward direction. In the $\langle 111 \rangle$ peak the contribution is about 20%. The modeling of channeling is not straightforward and the values given may be questioned.

The total contribution (including both directions) of the replacement, focused and of all collision chains to the modified recoil flux at the markers is 23, 26, and 64%. The collision chains also contribute to directions other than the low-index $\langle 100 \rangle$, $\langle 110 \rangle$, and $\langle 111 \rangle$ directions. Moreover, the momentum jump from one atomic row to another is possible and was already indicated by the early molecular dynamics calculation.³² Table V presents the average contributions of $\langle 100 \rangle$, $\langle 110 \rangle$, and $\langle 111 \rangle$ sequences to the $\langle 100 \rangle$ and $\langle 110 \rangle$ peaks in the backward direction. The fraction of the $\langle 110 \rangle$ chains in the $\langle 100 \rangle$ and $\langle 110 \rangle$ peaks is higher than that of the $\langle 100 \rangle$ sequences in the $\langle 100 \rangle$ and $\langle 110 \rangle$ peaks. This is explained, among other things, by the fact that four $\langle 110 \rangle$ axes, but only a single $\langle 100 \rangle$ axis, intersect the $\langle 100 \rangle$ plane that is parallel to the surface. The contribution of $\langle 111 \rangle$ sequences is, however, small compared to the $\langle 100 \rangle$ and $\langle 110 \rangle$ peaks.

D. Effect of thermal vibrations on the collision cascades and sequences

The effect of thermal vibrations on collision cascades and anisotropies is studied by repeating some of the calculations in the case of a static lattice. The projected range of Ar ions increases by a factor of 2 when thermal vibrations are neglected. This is due to the channelled ions for which penetration depth increases significantly. The depth distribution of the ions has a maximum at the depth $z \approx 20 \text{ \AA}$ as in the case of thermal vibrations, though the distribution has a more persistent tail than in Fig. 2(a). Thermal vibrations have practically no effect on the energy-loss curve. The tail of the current J is more persistent than in Fig. 2(b). The maximum of J is at an equal depth to that in the case of

thermal vibrations. Figure 8 shows the contributions of different generations of the first recoil in a replacement [Fig. 8(a)] and focused [Fig. 8(b)] chain. Thermal vibrations are omitted, whereas the other model parameters are equal to those in Fig. 5. The distributions in Fig. 8(a) are quite similar to those in Fig. 5(a). In the case of focused chains, the curve corresponding to the $\langle 110 \rangle$ direction is more peaked than in Fig. 5(b). Moreover, the tail in the distribution of the $\langle 110 \rangle$ direction in Fig. 5(b) has practically disappeared. This is explained, among other things, by the fact that when thermal vibrations are included, such collision sequences are feasible, where the first collisions are focused and subsequent ones defocused. These defocused collisions can again change to focused ones. This kind of complicated mechanism leads to the tail in Fig. 5(b). When thermal vibrations are omitted, the transition from focused to defocused collisions is improbable and thus the generation of the first recoil is quite small ($g \sim 2-4$).

The chains get longer when thermal vibrations are omitted. In the case of $\langle 110 \rangle$ focused sequences in the backward direction and at the depth $z=0.9 \text{ \AA}$, the mean length has increased by a factor of about 3. For the $\langle 100 \rangle$ and $\langle 111 \rangle$ chains the changes in the mean lengths are not so pronounced as for the $\langle 110 \rangle$ ones. The omission of thermal vibrations markedly increases the contributions of $\langle 110 \rangle$ focused and replacement sequences with lengths $L \geq 15 t_{uvw}$, e.g., in the case of the latter ones by a fac-

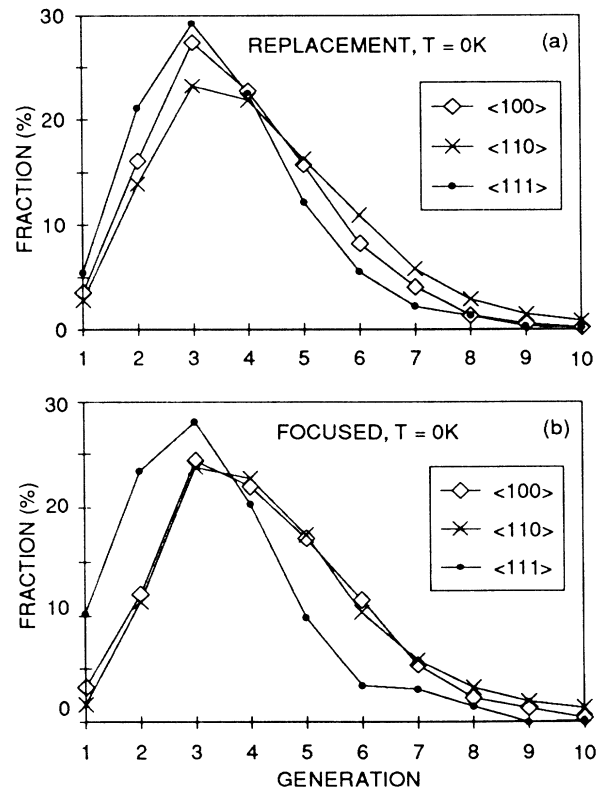


FIG. 8. Generation of the first recoil in a replacement (a) and focused (b) chain. The marker is at the depth $z=0.9 \text{ \AA}$ and recoils move in the backward direction. The target temperature is 0 K.

tor of over 4. The total fraction of all focused chains increases almost 30% in the backward direction and at the depth $z=0.9 \text{ \AA}$ when the temperature is 0 K. For other types of chains the changes are about 10%. The total contribution of focused sequences is higher than that of defocused ones when thermal vibrations are omitted. At the temperature 300 K the situation was the opposite.

Thermal vibrations have a pronounced role when the contribution of focused sequences to the $\langle 110 \rangle$ peaks is studied. The fraction in this case (without thermal vibrations) is 75% on average in the backward direction, i.e., it is about 40% higher than at the temperature 300 K. In other cases the effect of thermal vibrations is markedly smaller, the differences in the contributions at two temperatures being about 10%. The distributions of different contributions to the $\langle 100 \rangle$ and $\langle 110 \rangle$ peaks are qualitatively similar to those in Fig. 7 and therefore are not presented. The large decrease in the contribution of focused sequences to the $\langle 110 \rangle$ peaks when thermal vibrations are included is accounted for by the fact that they hamper a focused transfer of momentum along the $\langle 110 \rangle$ rows. This all indicates that thermal vibrations must be included in realistic model calculations.

VII. CONCLUSIONS

The distributions of the recoil vector fluxes have been studied in order to investigate the evolution of the collision cascade anisotropies. The parameters that well reproduce the experimental sputtering data have been used. This paper clearly shows that collision cascades in Cu(100) bombarded by 5-keV Ar ions are strongly anisotropic. The development of the collision cascade is entirely governed by the crystal structure. The cascades are backward directed near the surface and they become gradually forward directed deeper in the target. The modified recoil vector flux distributions N_r^m are dominated by the $\langle 110 \rangle$ peaks in the backward direction. In addition to these peaks, there are smaller $\langle 100 \rangle$ and $\langle 111 \rangle$ peaks. In the backward direction the depth dependence of the N_r^m distributions is insignificant. In the forward

direction the $\langle 110 \rangle$ peaks start to develop near the surface ($z \approx 6.3 \text{ \AA}$) and become more pronounced deeper in the target. In addition to this, there are also smaller $\langle 100 \rangle$ and $\langle 111 \rangle$ peaks. The N_r^m distributions are dominated by the $\langle 110 \rangle$ peaks in both directions even at a depth of the order of twice the projected range of the incoming ions. The energy resolution of the N_r^m distribution shows that the $\langle 110 \rangle$ peaks develop at lower and the $\langle 100 \rangle$ and $\langle 111 \rangle$ peaks at higher energies.

The linear collision sequences are the principal mechanism behind the $\langle 100 \rangle$ and $\langle 110 \rangle$ peaks. The replacement and focused chains make the most prominent contribution to the $\langle 110 \rangle$ peaks, while in the case of the $\langle 100 \rangle$ peak the fractions of the replacement and defocused chains are highest. The role of the collision sequences to the $\langle 111 \rangle$ peak is not so pronounced as to the $\langle 100 \rangle$ and $\langle 110 \rangle$ peaks. All collision chains also make a major contribution to the N_r^m distributions. Defocused and focused sequences are the principal mechanism for the N_r^m distributions. The fraction of the replacement chains is somewhat smaller. Collision sequences propagate most frequently along the $\langle 110 \rangle$ rows, the $\langle 111 \rangle$ chains making the lowest contribution. The collision sequences are mainly of the short-range type, except the $\langle 110 \rangle$ replacement and directional ones. The number of collisions needed to initiate a collision chain is usually quite small, though in the case of $\langle 110 \rangle$ focused and defocused sequences a diversity of mechanisms exists because such a chain can also be created after several collisions.

Thermal vibrations have an appreciable effect on the collision sequences and should be included in realistic model calculations. The lengths of the chains are higher in the case of a static lattice than when the thermal vibrations are included. Defocused sequences, however, are an exception. The thermal vibrations effectively hamper a focused transfer of momentum along an atomic row and result in attenuation of focused chains. The contributions of replacement and directional collision sequences also decrease in the case of nonzero temperature. Only the fraction of defocused chains is increased.

¹P. Sigmund, *Rev. Roum. Phys.* **17**, 823 (1972); **17**, 969 (1972); **17**, 1079 (1972).

²P. Sigmund, in *Sputtering by Particle Bombardment I*, edited by R. Behrisch (Springer-Verlag, Berlin, 1981), pp. 9-72.

³J.B. Sanders and H.E. Roosendaal, *Radiat. Eff.* **24**, 161 (1975).

⁴U. Littmark and P. Sigmund, *J. Phys. D* **8**, 241 (1975).

⁵U. Littmark and W.O. Hofer, *Nucl. Instrum. Methods* **168**, 329 (1980).

⁶H.E. Roosendaal, U. Littmark, and J.B. Sanders, *Phys. Rev. B* **26**, 5261 (1982).

⁷H.M. Urbassek, *Nucl. Instrum. Methods B* **4**, 356 (1984).

⁸K.T. Waldeer and H.M. Urbassek, *Nucl. Instrum. Methods B* **18**, 518 (1987).

⁹R.H. Silsbee, *J. Appl. Phys.* **28**, 1246 (1957).

¹⁰R.S. Nelson, M.W. Thomson, and H. Montgomery, *Philos. Mag.* **7**, 1385 (1962).

¹¹M.W. Thompson, *Phys. Rep.* **69**, 335 (1981).

¹²M. Hou and W. Eckstein, *Max-Planck-Institut für Plasma-physik*, Report No. IPP 9/65, 1988 (unpublished).

¹³V.I. Shulga, *Radiat. Eff.* **70**, 65 (1983); **82**, 169 (1984); **84**, 1 (1985).

¹⁴M. Hou and W. Eckstein, *Nucl. Instrum. Methods B* **13**, 324 (1986).

¹⁵Y. Yamamura and W. Takeuchi, *Nucl. Instrum. Methods B* **29**, 461 (1987).

¹⁶W. Eckstein and M. Hou, *Nucl. Instrum. Methods B* **31**, 386 (1988).

¹⁷M. Posselt, *Nucl. Instrum. Methods B* **36**, 420 (1989).

¹⁸M. Hautala and H.J. Whitlow, *Nucl. Instrum. Methods B* **6**, 466 (1985).

- ¹⁹H.J. Whitlow and M. Hautala, Nucl. Instrum. Methods B **18**, 370 (1987).
- ²⁰M. Hautala and J. Likonen, Phys. Rev. B **41**, 1759 (1990).
- ²¹J. Likonen, Phys. Rev. B **42**, 3853 (1990), following paper.
- ²²M. Hautala, Phys. Rev. B **30**, 5010 (1984).
- ²³J. Likonen and M. Hautala, J. Phys. Condens. Matter **1**, 4697 (1989).
- ²⁴J. Likonen and M. Hautala, Appl. Phys. A **45**, 137 (1988).
- ²⁵M.T. Robinson, in *Sputtering by Particle Bombardment I*, edited by R. Behrisch (Springer-Verlag, Berlin, 1981), pp. 73-144.
- ²⁶O.S. Oen and M.T. Robinson, Nucl. Instrum. Methods **132**, 647 (1976).
- ²⁷M.T. Robinson and I.M. Torrens, Phys. Rev. B **9**, 5008 (1974).
- ²⁸P. Sigmund, A. Oliva, and G. Falcone, Nucl. Instrum. Methods **194**, 541 (1982).
- ²⁹R.S. Nelson and M.W. Thompson, Proc. R. Soc. London, Ser. A **259**, 458 (1961).
- ³⁰D.E. Harrison, Jr., N.S. Levy, J.P. Johnson III, and H.M. Effron, J. Appl. Phys., **39**, 3742 (1968).
- ³¹M.W. Thompson, in *The Interaction of Radiation with Solids*, edited by R. Strumane, J. Nihoul, R. Gevers, and S. Amelinckx (North-Holland, Amsterdam, 1964), pp. 84-113.
- ³²J.B. Gibson, A.N. Goland, M. Milgram, and G.H. Vineyard, Phys. Rev. **120**, 1229 (1960).

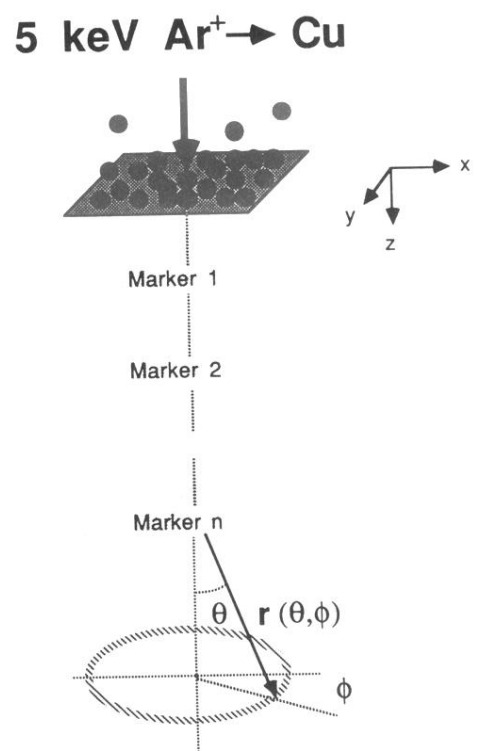


FIG. 1. Schematic illustration of the geometry used in the simulations.